

Classification of diffusion modes in single particle tracking data: feature based vs. deep learning approach

Patrycja Kowalek, Hanna Loch-Olszewska, and Janusz Szwabiński

Faculty of Pure and Applied Mathematics, Hugo Steinhaus Center, Wrocław University of Science and Technology

Single-particle trajectories measured in microscopy experiments contain important information about dynamic processes undergoing in a range of materials including living cells and tissues. However, extracting that information is not a trivial task due to the stochastic nature of particles' movement and the sampling noise. In this paper, we adopt a deep learning method known as a convolutional neural network (CNN) to classify modes of diffusion from given trajectories. We compare this fully automated approach working with raw data to classical machine learning techniques that require data preprocessing and extraction of human-engineered features from the trajectories to feed classifiers like random forest or gradient boosting. All methods are tested using simulated trajectories for which the underlying physical model is known. From the results it follows that although the feature-based methods perform better than CNN in terms of accuracy and are computationally cheaper, the performance of CNN is already very good and may be probably improved after carrying out an expanded search for the best performing CNN model on an HPC platform.

Keywords: single particle tracking, diffusion modes, machine learning, deep learning

I. INTRODUCTION

Recent advances in single-molecule microscopy and imaging technologies have made single-particle tracking (SPT) a popular method for analyzing dynamic processes in a range of materials [1, 2]. In a typical SPT measurement the molecules of interest (e.g. proteins in a living cell) are tagged with fluorescent dye particles. Once the sample is illuminated by a laser, the labels produce light, their positions are determined with a microscope and a snapshot is taken. Using lasers that flash at short time intervals allows for tracking of the movement of the molecules over time. The recorded positions are then used to reconstruct trajectories of individual molecules. These trajectories are then analyzed in order to extract local physical properties of the molecules and their environment, such as velocity, diffusion coefficient (or tensor) and confinement (local density of obstacles) [3].

The SPT method is of particular importance for fundamental biology. It bridges the gap between biology, biochemistry and biophysics and allows for at least a partial understanding of living cells on a microscopic basis. It helped already to unveil the details of the movement of molecular motors inside cells [4, 5] or target search mechanisms of nuclear proteins [6].

The analysis of SPT trajectories is not a trivial task due to the stochastic nature of the molecules' movement. It usually starts with the detection of a corresponding motion type of a molecule, because this information may already provide insight into mechanical properties of the molecule's surrounding [7]. Four basic types of motion are observed in SPT experiments: normal diffusion (ND) [8], directed motion (DM) [9–11], anomalous diffusion (AD) [12] and confined diffusion (CD) [13]. The most common analysis method uses mean square displacement (MSD) curves [11]. Within this approach one fits the theoretical curves for various physical models to the data and then selects the best fit with statistical analysis [13]. However, in many cases the actual trajectories are too short for extracting a meaningful information from the time-averaged MSDs. Moreover, the finite localization precision adds a term to the MSD, which can limit the interpretation of the data [11, 14, 15]. Consequently, several alternative methods have been introduced to overcome these problems. For instance, the full distribution of displacements may be fitted to a mixed model in order to extract differences in diffusive behavior between subsets of particle ensembles [16]. The moment scaling spectrum method can also be used to categorize various modes of motion [17, 18]. The distribution of directional changes [19], the mean maximum excursion method [20] and the fractionally integrated moving average (FIMA) framework [21] may efficiently replace the MSD estimator for classification purposes. Hidden Markov Models (HMM) has been proposed to check the heterogeneity within single trajectories [22, 23]. They also have proven to be quite useful in the detection of confinement [24].

An alternative approach to an analysis of trajectories rooted in computer science and statistics is also possible. In recent years we are witnessing an exciting development in machine learning (ML) methods. Due to algorithmic advances combined with increased data availability and more powerful computers machine learning may already outperform human experts at some tasks including classification, i.e. the problem of identifying to which category a new observation belongs on the basis of a training dataset containing observations with a known category membership. Since the detection of the motion falls into the domain of classification, one may try to tackle this problem with machine learning algorithms. This approach is very appealing, because it would enable an automated analysis of many hundreds or even thousands of trajectories with a reduced amount of manual intervention and initial data curation.

Several attempts to analyze SPT trajectories with ML methods have been already carried out. For instance, Monnier et al [13] used Bayesian approach to MSD-based classification of motion modes. Dosset and coworkers [25] used a simple back-propagation neural network to discriminate between different types of diffusion. Wagner et al [26] built a random forest classifier for normal, anomalous, confined and directed diffusion. Although each of these attempts uses a different machine learning classification algorithm, they all belong to the class of feature based methods. Each trajectory within this approach is described by a set of human-engineered features and only those features were provided as input to a classifier model. In contrast, deep learning methods extract features on their own from raw data, without any effort from human expert. They are gaining on popularity in recent years and were already successfully applied to computer vision [27–29], speech recognition [30, 31] and natural language processing [32, 33].

One of the most popular deep learning methods are convolutional neural networks (CNN) [34], which excels in image classification. They have been already applied to single-particle recognition in microscopy experiments [35, 36]. However, although some attempts to time series analysis with CNNs are already known [37–39], to the best of our knowledge they have not been applied yet to the problem of classification of motion types from raw trajectories.

Thus, the goal of this paper is to propose a novel approach to SPT trajectory classification based on the CNN deep learning method and to compare its performance with two popular feature-based methods: random forests [40, 41] and gradient boosting [42]. Since all of these methods require large training datasets with trajectories labeled already with a corresponding motion type, we will use synthetic data to train and validate the models. As for the traditional methods, we will follow the approach of Wagner et al [26] and use their set of features for classification purposes.

The paper is divided as follows. In Sec. II we introduce basic types of diffusion and briefly discuss the mean square

displacement curves as a common tool of trajectory analysis. Classification methods are introduced in Sec. III. In Sec. IV we summarize methods for computer generation of synthetic trajectories used as training and validation data. Features used by the traditional classification methods are introduced in Sec. V. Results of our analysis are presented in Sec. VI, followed by some concluding remarks.

II. DIFFUSION MODES AND THEIR ANALYSIS

The observed SPT trajectories can be classified into four basic motion types: normal diffusion (ND) [8], directed motion (DM, also known as diffusion with flow) [9–11], anomalous diffusion (AD) [12] and confined diffusion (CD) [13].

Normal diffusion is characterized by a Gaussian probability density function, whose variance increases linearly in time [8]. It takes place when a particle moves completely unrestricted and is often described as resulting from microscopic random walks with independent and identically distributed steps. The process is described by the Fick's law [43].

The term “anomalous diffusion” has been coined to label geometrically unrestricted diffusion processes that deviate from the Fick's law [44, 45]. It was found in many systems including ultra-cold atoms [46], telomeres in the nucleus of cells [47], ion channels in the plasma membrane [48], colloidal particles in the cytoplasm [49] and worm-like micellar solutions [50]. AD has been proposed as a measure of crowding in the systems like cytoplasm [51].

Confined diffusion refers to particles' motion restricted to bounded domains [52]. It was found in the movement of receptors on cell membranes [53–55], protein diffusion inside the cell nucleus [56] or transporter diffusion through nuclear pores [57, 58]. As far as the living cells are concerned it was observed that the confinement may result from corrals formed by cytoskeletal proteins or from restrictions to motion imposed by lipid domains [59]. Within such corrals a particle diffuses freely and the barriers are usually reflective.

Directed motion [9] may be understood as a combination of two processes: normal diffusion and convection. There are already several models trying to explain the mechanism behind this type of motion. In the uniform flow model for instance it is assumed that an entire membrane moves with a constant velocity and a particle diffuses with respect to the membrane [60, 61]. In the conveyor belt model a mobile particle is reversibly attached to a cytoskeletal motor [60–64]. When it is bound, it moves with a constant velocity along a cytoskeletal element. When it is unbound, it diffuses freely.

A standard way of identifying different diffusion modes is based on the analysis of the mean square displacement (MSD) of particles [65]. The MSD is defined as

$$MSD \equiv \langle (X(t) - X(0))^2 \rangle = \frac{1}{M} \sum_{j=1}^M (X_j(t) - X_j(0))^2, \quad (1)$$

where $X_j(t)$ is the position of the j -th particle after time t and M is the number of particles (i.e. independent trajectories). For the sake of convenience we will usually assume $X(0) = 0$ in our considerations. Thus, MSD is nothing but an ensemble average of the square displacement over the probability distribution of $X(t)$. However, due to a limited number of trajectories in many single particle tracking experiments, the ensemble averaged MSD is usually replaced by the time averaged MSD (TAMSD) calculated from a single trajectory. Given a trajectory in form of N consecutive two dimensional positions $X_i = (x_i, y_i)$ ($i = 1, \dots, N$) recorded with a constant time interval Δt , the TAMSD at time lag $n\Delta t$ is defined as

$$\rho(n\Delta t) = \frac{1}{N-n} \sum_{i=1}^{N-n} (X_{i+n} - X_i)^2. \quad (2)$$

It is worth to mention that for an ergodic process with stationary increments the TAMSD converges to the ensemble averaged MSD in the limit $N \rightarrow \infty$.

According to Saxton [14], for the four basic modes of diffusion we have:

$$\begin{aligned} \rho_{ND}(n\Delta t) &= 4Dn\Delta t, \\ \rho_{AD}(n\Delta t) &= 4D(n\Delta t)^\alpha, \\ \rho_{DM}(n\Delta t) &= 4Dn\Delta t + (vn\Delta t)^2, \\ \rho_{CD}(n\Delta t) &\simeq r_c^2 \left[1 - A_1 \exp\left(\frac{-4A_2 D n \Delta t}{r_c^2}\right) \right]. \end{aligned} \quad (3)$$

Here, $\alpha < 1$ is the anomalous exponent, v is the velocity in the directed motion, the constants A_1 and A_2 characterize the shape of the confinement and r_c is the confinement radius.

For pure trajectories with no localization errors one could actually determine their diffusion modes simply based on the shapes of MSD curves and their mathematical models given by Eq. (3). However, in case of real trajectories there is usually a lot of noise in the data, which makes the fitting of a mathematical model a challenging task, even in the simplest case of the normal diffusion [11]. Moreover, according to Eq. (2), only the MSD values corresponding to small time lags are well averaged. The larger the lag is the smaller the number of displacements contributing to the averages, resulting in fluctuations increasing with the lag. This constitutes a problem in particular in case of short trajectories, for which the fit to mathematical models has to be limited to just a few first time lags. Finally, the displacements in Eq. (2) are not independent from each other. Although other definitions of TAMSD using only nonoverlapping displacements are possible, they all reduce the number of terms in each average, again resulting in much noisier MSD curves. This is the reason why we are interested in classification methods that go beyond fitting of mathematical models to the MSD curves.

III. CLASSIFICATION METHODS

As already mentioned in the introduction, there are two approaches to automatic data classification. Traditional machine learning is a set of methods of statistical learning where each instance in a dataset is described by a set of human-engineered features or attributes [66]. In contrast, deep learning methods extract features from raw data without any effort from human expert [67]. The representation of data is constructed automatically and there is no need for complex data preprocessing as in the case of the machine learning.

After many successful applications in different areas [27–33] the deep learning approach constitutes nowadays the state-of-the-art technology for automatic data classification and overshadows a little bit the classical machine learning algorithms. However, in some specific situations the latter ones are still better to use. The reason is at least threefold: they work better on small data, are financially and computationally cheaper and usually are easier to interpret. Thus the ultimate goal of this paper is to compare the performance of machine and deep learning algorithms applied to the recognition of the diffusion type in single particle tracking data. We will examine two classical algorithms, i.e. random forests [40, 41] and gradient boosting [42], together with convolutional neural networks (CNN) [34] being one of the most popular deep learning methods. In the remaining part of this section we will briefly introduce them.

A. Feature based methods

Both random forests and gradient boosting algorithms belong to the class of ensemble learning, i.e. methods that generate many classifiers and aggregate their results. In both cases, decision trees [68] are used as the basic classifier.

Decision trees are a data mining method used very often for classification purposes. A decision tree depicts rules for dividing existing data into groups based on values of selected features. The first rule splits the entire data set into some number of subsets and then another rules may be applied to each of those subsets forming a next generation of them. The procedure is repeated until the data in each subset forms a final group.

Finding a proper attribute to split the data is not a trivial task. For instance, in the iterative dichotomiser 3 (ID3) method invented by Ross Quinlan [69] a feature with the highest information gain is selected for the next split. Here, the information gain is defined as the difference between the Shannon entropy before and after the separation of data.

Decision trees are easy to understand and interpret. They constitute one of the best approaches to identify most significant features and the relationships between them. And they usually do not require a data preprocessing, because they are able to handle missing data and are not influenced by outliers. However, they are unstable in the sense that a small variation in the data may lead to a completely different tree [70]. And they have the tendency to overfit, i.e. they correspond to closely or exactly to a particular set of data, and may therefore fail to fit additional data or predict future observations reliably [71]. Although methods like pruning are known to avoid overfitting, it is the main reason why the decision trees are used as building blocks of ensemble classifiers rather than standalone ones.

1. Random forests

In a random forest, several decision trees are constructed from the same training data. For a given input, the predictions of individual trees are aggregated and then their mode is outputted as the class of the input data. A modern version of the algorithm combines the bagging idea proposed by Breiman [41] with the random subspace method invented by Ho [40, 72]. Bagging repeatedly selects a random sample with replacement of the training set and fits trees to these samples. In order to avoid correlations between the trees, for each one a random subset of features is selected. Typically, in a classification problem with N features, \sqrt{N} of them are used to build one tree.

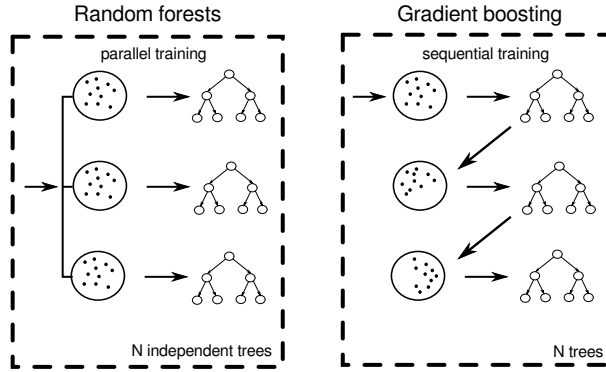


FIG. 1. Comparison between random forest (left) and gradient boosting methods (right). In the random forest, N independent learners (trees) are built in parallel from random subsets of the input data set. In gradient boosting, the next tree is constructed from the pseudo-residuals of the ensemble and added to it.

2. Gradient boosting

Although other choices are possible, gradient boosting is typically used with decision trees of a fixed size as base learners. In contrast to random forests, the trees in boosting are not independent. Instead, the single classifiers are built sequentially by learning from mistakes committed by the ensemble [42, 73] (see Fig. 1 for a schematic comparison of the two methods).

The basic principle of the gradient boosting is simple. We start with a single tree fitted to the input data set. Then, in every step we check the output of the classifier and compute pseudo-residuals, e.g. the negative gradient of the cross entropy [74]. A new tree is trained on those residuals and added to the ensemble.

B. Deep learning methods

Deep learning (DL) methods have taken their inspiration from biological nervous systems. They are very appealing as a tool for classification tasks, because they operate on raw data. They do not require any feature selection and extraction carried out by a human expert. Instead, they use a cascade of multiple layers of nonlinear processing units for feature identification, extraction and transformation in order to learn multiple levels of data representations [75].

In this paper, we are going to use convolutional neural networks for trajectory classification. They have been already successfully applied to many tasks including a time series analysis [76]. A schematic architecture of a CNN is shown in Fig. 2. Such a network has usually two components. The one consisting of hidden layers is responsible for extraction of features from the raw input data. The layers will perform a series of convolutions and pooling operations during which attributes of data are detected. Each convolution uses a different filter which is sliding over the input and producing its own feature map in form of a 3D array. All the maps are then combined together as the final output of the component. The role of pooling is to reduce the dimensionality of feature maps in order to decrease the number of parameters and computations in the network. The classification part contains few fully connected layers like a regular neural network [77]. Flattening of data is usually required at the interface between the components, because the fully connected layers can process only 1D vectors.

IV. SYNTHETIC DATA

All three methods described in the previous section belong to the class of supervised learning, i.e. they infer a model from a set of training examples [78]. Each sample is a pair consisting of an input object (a trajectory) and a desired output value (a diffusion mode). The model is a function that maps an input to an output and can be used for classification of new input data.

Since thousands of labeled trajectories are needed to train the classifiers, especially in the deep learning case, we will use computer-generated synthetic 2D trajectories as our training set. Simulation methods for every type of diffusion will be briefly discussed below.

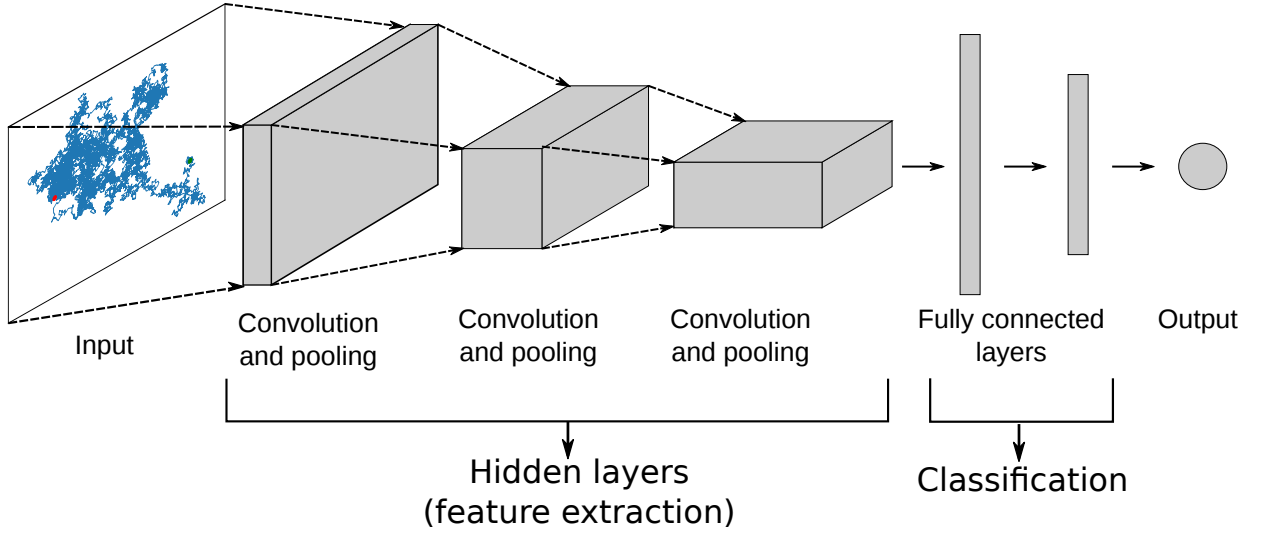


FIG. 2. A schematic architecture of a CNN. The network consists of two components: hidden layers responsible for feature extraction from input data and fully connected layers carrying out the classification.

A. Normal diffusion

According to Michalet [11], the probability distribution of the displacement's norm in case of the normal diffusion is given by

$$F_d(u) = \frac{2u}{4D\Delta t} \exp\left(\frac{-u^2}{4D\Delta t}\right), \quad u \geq 0 \quad (4)$$

where Δt is the time interval during which the displacement is recorded. Mathematically, Eq. (4) is a Rayleigh distribution [79]. To simulate a trajectory, we randomly choose a start position of a particle and a random direction of displacement α and then pick up a random steplength d from Eq. (4). We calculate the new position by adding the displacement to the start position,

$$\begin{aligned} x_{new} &= x_{old} + d \cos \alpha, \\ y_{new} &= y_{old} + d \sin \alpha. \end{aligned} \quad (5)$$

The new coordinates become the starting point for the next step and the procedure is repeated a given number of times.

Inverse transform sampling [80] may be used to generate numbers with distribution given by Eq. (4). Calculating the CDF of the distribution and inverting it will yield the formula

$$x = \sqrt{-4D\Delta t \ln(1-y)}, \quad (6)$$

which can be used to transform from a uniformly distributed variable y to a variable x following the Rayleigh distribution.

B. Directed motion

Once we have a procedure generating a normal diffusion trajectory, simulation of the directed motion is straightforward. For a given velocity \vec{v} , in each step we simply calculate a correction to the position due to the active motion,

$$\begin{aligned} dx_i &= v\Delta t \cos \beta, \\ dy_i &= v\Delta t \sin \beta, \end{aligned} \quad (7)$$

and add it to the new coordinates:

$$\begin{aligned} x_{new} &= x_{old} + d \cos \alpha + dx_i, \\ y_{new} &= y_{old} + d \sin \alpha + dy_i. \end{aligned} \quad (8)$$

The angle β in Eq. (7) is the direction of the velocity.

Following Wagner et al [26], we may want to introduce a measure of how a trajectory is influenced by the active motion,

$$R = \frac{v^2 T}{4D}, \quad (9)$$

with T being the time duration. This measure can be helpful in generating similar trajectories with different values of v and D .

C. Confined diffusion

Again, a small modification of the normal diffusion procedure is needed to simulate a confined diffusion [26]. We assume that a particle starts from the center of a 2D circular reflective boundary. We divide every step of the simulation in 100 substeps with $\Delta t' = \Delta t/100$. In every substep we carry out a normal diffusion step. The position of the particle after the substeps will be updated only if the distance from the center to new coordinates is smaller than the radius of the reflective boundary.

Wagner et al [26] have introduced the boundedness parameter B , defined as the area of the smallest ellipse enclosing a normal diffusion trajectory (with no confinement) divided by the area of the confinement,

$$B = \frac{A_{ellipse}}{\pi r_c^2}. \quad (10)$$

From simulations it follows that $A_{ellipse} \simeq \pi D N \Delta t$. This leads to

$$B \simeq \frac{DN \Delta t}{r_c^2}. \quad (11)$$

As in the case of the directed motion, this parameter will help to evaluate trajectories independently of the actual values of D and r_c .

D. Anomalous diffusion

Anomalous diffusion was simulated with the fractional Brownian motion (FBM) [81]. We used a dedicated Python package called `fbm` for that purpose [82]. Davies-Harte algorithm [83] was utilized to generate realizations of FBM.

E. Adding noise

Real trajectories can be altered by various measurement noises such as localization errors, electronic noise, drift or vibrations of the sample or postprocessing errors [84]. To account for these issues, we added normal Gaussian noise with zero mean and the standard deviation σ to each simulated position.

Let us first introduce two different signal to noise ratios: one for ND, AD and CD,

$$SNR_1 = \frac{\sqrt{D \Delta t}}{\sigma}, \quad (12)$$

and another one for DM,

$$SNR_2 = \frac{\sqrt{D \Delta t + v^2 \Delta t^2}}{\sigma}. \quad (13)$$

Instead of setting σ directly in our simulations, we will prefer to set a random level of SNR first and then to calculate the standard deviation for given D and Δt from one of the above equations.

Parameter	Meaning	Range of values
Δt	timelag between steps	1/30
D	diffusion coefficient	9.02
N	length of a trajectory	30 – 600
B	boundedness	1 – 6
R	active motion to diffusion ratio	1 – 17
α	anomalous exponent	0.3 – 0.7
SNR	signal to noise ratio	1 – 9

TABLE I. Parameters of the simulation and their values. All parameters except Δt and D were randomly chosen from given ranges.

F. Simulation details

Our training data consists of 20000 synthetic trajectories, i.e. 5000 for each diffusion type. Following Wagner et al [26] we used fixed values for two of the parameters: $\Delta t = 1/30$ s and $D = 9.02 \mu m^2/s$. As for the timelag, it is a typical value in experimental setups. The value of the diffusion coefficient D corresponds to a freely diffusing nanoparticle with a diameter 50 nm in water at 22°C. Other parameters were chosen randomly. The length of a trajectory was randomly selected between 30 and 600 steps. The boundedness parameter B was chosen from the range from 1 to 6. Then, Eq. (11) was used to calculate the radius of confinement r_c . For the anomalous exponent α we took the values from 0.3 to 0.7, i.e. the typically observed range [14, 85, 86]. The factor R characterizing the directed motion was selected between 1 and 17. Having a value of R , we could calculate the corresponding velocity v of the active motion from Eq. (9). Finally, the signal to noise ratio was randomly chosen from 1 to 9. Depending on the diffusion type, Eq. (12) or Eq. (13) was used to determine the standard deviation σ .

All parameters and their values are summarized in Table I. We used our own codes written in Python [87] to simulate the training set. The codes are available upon request.

V. FEATURE EXTRACTION

As already mentioned in Sec. III, traditional machine learning methods like random forests or gradient boosting cannot work with raw trajectories. Instead, they expect low dimensional vectors of features characterizing the trajectories as input. It is the task of a human expert to provide meaningful features and to use them in order to prepare a representation of each trajectory in the training data.

For the purpose of this work we will follow the approach of Wagner et al [26] and use their nine features together with the diffusion coefficient fitted from the data as the tenth one. In this section we will give a short description of the features used for training of our classifiers.

A. Diffusion coefficient

We will use the diffusion coefficient of the model given by the first of Eqs. (3) fitted to the mean square displacement curve estimated by Eq. (2).

B. Anomalous exponent

Anomalous exponent α is the exponent in the second model defined in Eqs. (3). Again, it will be fitted to the MSD curve obtained from Eq. (2).

C. Asymmetry

In most of the cases an average behavior of a diffusing particle is expected to be symmetric. In case of a directed motion however the average tends to be highly asymmetric. The asymmetry can be thus used to detect directed motion among trajectories.

There are several possibilities for introducing a measure of asymmetry of a trajectory. Following Saxton [53] we will derive it from the gyration tensor, which describes the second moments of positions of a particle. For a 2D random walk of N steps it is given by

$$\mathbf{T} = \begin{pmatrix} \frac{1}{N} \sum_{j=1}^N (x_j - \langle x \rangle)^2 & \frac{1}{N} \sum_{j=1}^N (x_j - \langle x \rangle)(y_j - \langle y \rangle) \\ \frac{1}{N} \sum_{j=1}^N (x_j - \langle x \rangle)(y_j - \langle y \rangle) & \frac{1}{N} \sum_{j=1}^N (y_j - \langle y \rangle)^2 \end{pmatrix}, \quad (14)$$

where $\langle x \rangle = (1/N) \sum_{j=1}^N x_j$ is the average of x coordinates over all steps in the random walk. We will define the asymmetry as [88]

$$A = -\log \left(1 - \frac{(\lambda_1 - \lambda_2)^2}{2(\lambda_1 + \lambda_2)} \right), \quad (15)$$

where λ_1 and λ_2 are the principle radii of gyration, i.e. the eigenvalues of the tensor \mathbf{T} .

D. Efficiency

Efficiency relates the net squared displacement of a particle to the sum of squared step lengths,

$$E = \frac{|X_{N-1} - X_0|^2}{(N-1) \sum_{i=1}^{N-1} |X_i - X_{i-1}|^2}. \quad (16)$$

It is a measure for linearity of a trajectory and like asymmetry, it may help to detect directed motion.

E. Fractal dimension

In general, the fractal dimension is a measure of the space-filling capacity of a pattern that tells how a fractal scales differently from the space it is embedded in. According to Katz and George [89], the fractal dimension of a trajectory can be calculated as

$$FD = \frac{\log N}{\log(NdL^{-1})}, \quad (17)$$

where L is the total length of the path, N is the number of steps and d is the largest distance between any two positions.

The measure takes values around 1 for straight trajectories (direct motion), around 2 for random ones (normal diffusion) and around 3 for constrained trajectories (confined or anomalous diffusion) [89].

F. Gaussianity

Trajectory's gaussianity was introduced by Ernst et al [90] to check the Gaussian statistics on increments,

$$g(n) = \frac{\langle r_n^4 \rangle}{2\langle r_n^2 \rangle^2}, \quad (18)$$

where the trajectory's quatic moment is given by

$$\langle r_n^4 \rangle = \frac{1}{N-n} \sum_{i=1}^{N-n} |X_{i+n} - X_i|^4. \quad (19)$$

For normal diffusion we should get gaussianity equal to 0. Since we used FBM, which has Gaussian increments, to simulate anomalous diffusion, we expect to get the same result for AD. The other types of motion should show deviations from 0.

G. Kurtosis

Kurtosis measures the asymmetry and peakiness of the distribution of points within a trajectory [88]. For its calculation the position vectors X_i are projected onto the dominant eigenvector \vec{r} of the gyration tensor (14) yielding scalars

$$x_i^p = X_i \cdot \vec{r}. \quad (20)$$

Kurtosis is defined as the fourth moment of the set of x_i^p ,

$$K = \frac{1}{N} \sum_{i=1}^N \frac{(x_i^p - \bar{x}^p)^4}{\sigma_{x^p}^4}, \quad (21)$$

with \bar{x}^p being the mean projected position and σ_{x^p} - the standard deviation of x^p .

H. MSD ratio

The mean square displacement ratio characterizes the shape of the MSD curve. We will define it as follows:

$$MSDR(n_1, n_2) = \frac{\langle r_{n_1}^2 \rangle}{\langle r_{n_2}^2 \rangle} - \frac{n_1}{n_2}, \quad (22)$$

where $n_1 < n_2$. Taking Eq. (3) into account we see that $MSDR = 0$ for normal diffusion, it is negative for direct motion and positive for other types of diffusion. In our analysis we simply took $n_2 = n_1 + \Delta t$ and calculated an averaged ratio for every trajectory.

I. Straightness

Straightness is a measure of the average direction change between subsequent steps. Similar to efficiency it relates the net displacement to the sum of step lengths:

$$S = \frac{|X_{N-1} - X_0|}{\sum_{i=1}^{N-1} |X_i - X_{i-1}|}. \quad (23)$$

J. Trappedness

Trappedness is the probability that a diffusing particle with the diffusion coefficient D and traced for a time interval t is trapped in a bounded region with radius r_0 . According to Saxton [53] it can be estimated by

$$P(D, t, r_0) = 1 - \exp \left(0.2045 - 0.25117 \left(\frac{Dt}{r_0^2} \right) \right). \quad (24)$$

For practical reasons we will replace r_0 by the estimated half of the maximum distance between any two positions. For D we will take its short-time estimate, fitted to the first two points of the MSD curve.

VI. RESULTS

We decided to use existing libraries for the purpose of that project. Random forest and gradient boosting implementations available in `scikit-learn` [91], the most popular ML learning library in Python, were used to build the feature-based classifiers. And we used `mcfly` [92], a deep learning library for time series processing, to find and train a deep classifier working with raw diffusion data. All codes were written in Python and are available on request. The computations were carried out on an ordinary of-the-shelf workstation with Intels 8 core i7-6700 3.4 GHz CPU and 8 GB RAM. If not stated otherwise, the synthetic trajectories were randomly split into two subsets: a training set containing 70% of them and a test set.

	Random Forest	Gradient boosting
number of trees	500	500
maximum depth of a single tree	20	10
minimum number of samples required to split an internal node	2	5
minimum number of samples required to be at a leaf node	1	4

TABLE II. Optimal parameters for the random forest and gradient boosting models trained on our data. A randomized search method was used to determine those values.

	Random forest	Gradient boosting
Single split of data	96.43%	96.97%
10-fold cross validation	96.23%	96.47%

TABLE III. Accuracies of the feature based classifiers.

A. Featured based classification

The random forest classifier implemented in `scikit-learn` follows the original paper by Breiman [41]. The gradient boosting algorithm available in this library was described in Refs. [42, 93]. The parameters of the models were optimized with a randomized search method (the `RandomizedSearchCV` function in `scikit-learn`). They are summarized in Table II.

1. Accuracy

One of the basic metrics used to asses the performance of classification models is accuracy, defined as

$$acc = \frac{\text{number of correct predictions}}{\text{total number of predictions}}. \quad (25)$$

In Table III, accuracies for both feature-based classifiers are shown. The numbers in the first row correspond to the accuracy achieved after a single random split into training and test sets. For the second row we used the 10-fold cross validation method. The idea behind this technique is to randomly split the data set into 10 folds without replacement and use 9 of them for training and one for testing of the model. The procedure is repeated 10 times, so we obtain 10 models and accuracy estimates. An average of those estimates gives the overall accuracy.

Since in the gradient boosting an ensemble of the decision trees was built with the purpose to reduce the total error (see Sec. III for details), we would expect that the algorithm performs much better than the random forest. From Table III it follows, that its accuracy is indeed higher, but the differences are actually negligible. Both classifiers perform excellent with an average accuracy of more than 96%.

In Fig. 3, confusion matrices of the classifiers are presented. We see that in both cases, the classifiers made a total of 6000 predictions (sum of all matrix elements), including 1500 for each type of diffusion (sum of all elements in a matrix row). As far as the random forest model is concerned, the best performance was observed for the directed diffusion - among the 1500 directed trajectories only one was wrongly classified as an anomalous one. The performance decays slightly for the anomalous and confined modes and is significantly worse for the normal diffusion. The gradient boosting model reveals similar characteristics with slightly different absolute numbers.

The data collected in the confusion matrices may be used to generate a more detailed description of the performance of the models under investigation. The results are briefly summarized in Table IV. Here, we adopted two quantities commonly used in classification problems: precision and recall [94]. Precision is the fraction of correct predictions among all predictions. It tells us how often a classifier is correct if it predicts a given class. Recall is the fraction of correct predictions of a given class over the total number of members of this class. Despite small differences in the numbers, each of our models is characterized by both very high precision and recall. Thus, they not only return much more relevant results than the irrelevant ones (high precision), but also yield most of the relevant results (high recall).

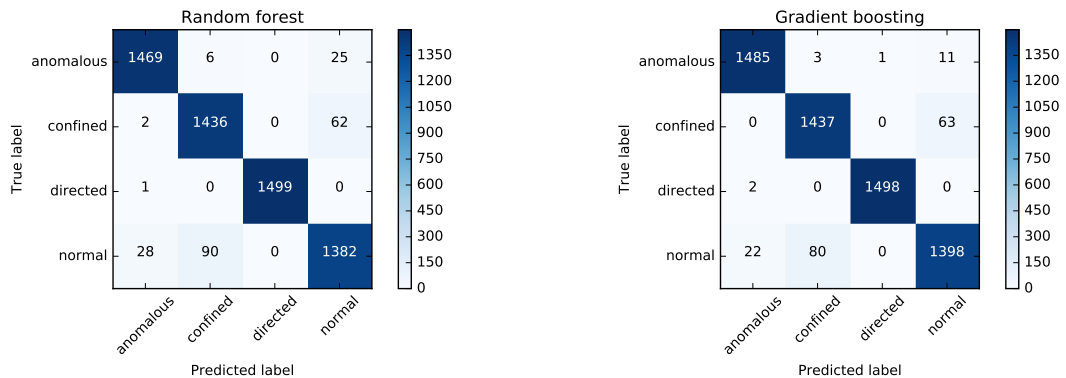


FIG. 3. (Color online) Confusion matrices for the random forest (left) and gradient boosting(right) classifiers.

	Random forest			Gradient boosting		
	precision	recall	support	precision	recall	support
anomalous	0.9793	0.9793	1500	0.9841	0.9900	1500
confined	0.9373	0.9573	1500	0.9454	0.9580	1500
directed	1.000	0.9993	1500	0.9993	0.9987	1500
normal	0.9408	0.9213	1500	0.9497	0.9320	1500
average/total	0.9643	0.9643	6000	0.9697	0.9697	6000
accuracy	96.43%			96.97%		

TABLE IV. A brief summary of the performance of feature based classifiers.

2. Feature importances

A nice detail of the ensemble classification methods is that they usually allow one to easily compute the relative importances of features for a given problem. Variables with high importance scores are the drivers of the outcome and their values have a significant impact on the correctness of a prediction. Features with low importance might be usually omitted from a model, making it faster to fit and predict.

The `scikit-learn` implementations of the random forest and gradient boosting classifiers calculate the importances on the fly during the training process and provide an interface to access them. Results are shown in Fig. 4. The linear diffusion coefficient D seems to be the most important feature in both cases, followed by the MSD ratio, straightness, efficiency and the anomalous exponent α . There are some differences between the methods as well. For instance, the dominance of the diffusion coefficient over all other features is less pronounced in the random forest. Instead, we observe non-vanishing importances of the remaining features, i.e. trappedness, asymmetry, kurtosis, fractal dimension and gaussianity. In contrast, the importances of those features are negligible in the gradient boosting case and the difference between the first and the second rank (diffusion coefficient and MSD ratio, respectively) is much higher.

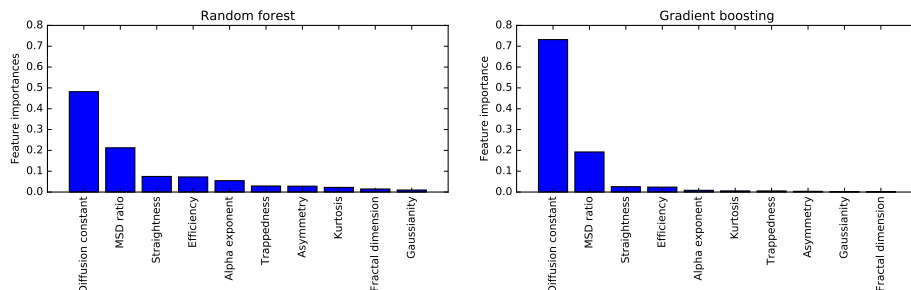


FIG. 4. Feature importances in the random forest (left) and gradient boosting (right) models.

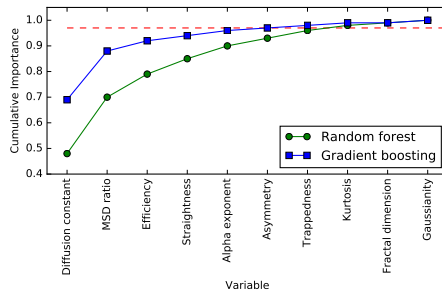


FIG. 5. Cumulative importance of features for both models. The red line is the 97% level of importance and indicates a threshold for feature selection.

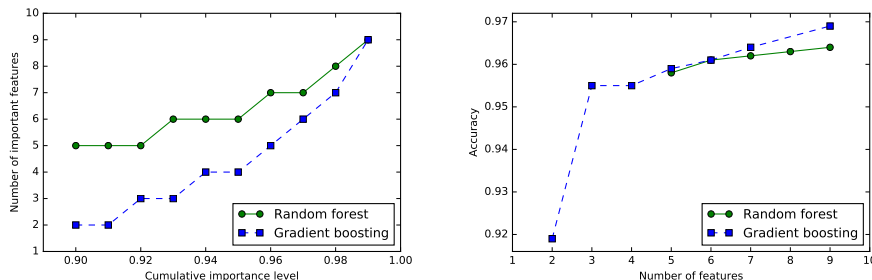


FIG. 6. Comparison of the feature based classifiers. Left plot: Number of features required to achieve given threshold of cumulative importance. Accuracy of classifiers trained with the reduced number of features.

To illustrate the differences between the models, in Fig. 5 we show the cumulative importances of features. The dashed horizontal line in this plot is the 97% level of importance and could indicate a threshold for feature selection, i.e. once the level is reached, we can omit the remaining features without affecting the model very much. In order to find a value of the threshold, one should check how his model generalizes to unseen data after removing attributes for different thresholds and then chose the one not negatively affecting the accuracy of the model.

To elaborate on that issue, we first found the feature selection thresholds for cumulative importance levels ranging from 90% up to 99%. Then we trained both models again with the reduced number of features as indicated by the threshold. Results are presented in Fig. 6. As we see, gradient boosting reaches a given cumulative importance level with a smaller feature set than the random forest. Consequently, it requires less features to achieve high accuracies.

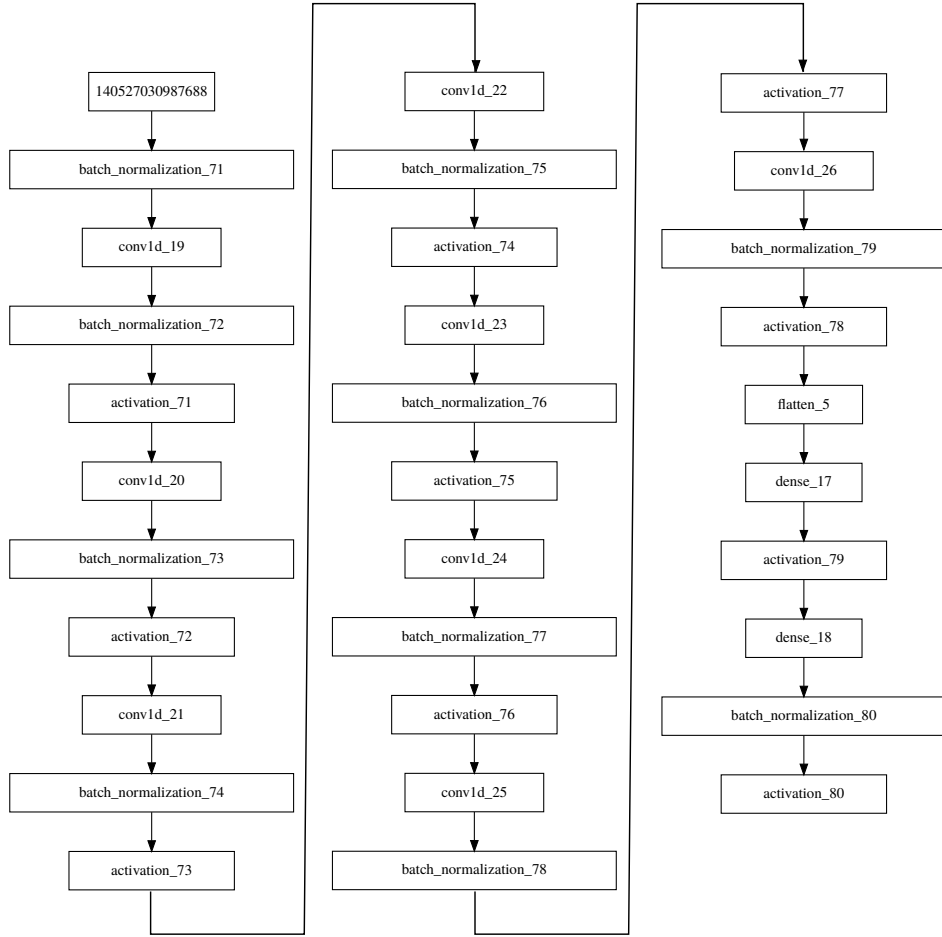
B. Deep learning classification

The `mcfly` package [92] used for the deep learning approach is a piece of software tailor-made to a classification of time series. One of its biggest advantages is a low entry level, because it does not require a user to define exactly the architecture of a convolutional neural network and to provide all hyper-parameters of the model. Instead, it carries out a search over a suitable architectures and provides all hyper-parameters to find the best performing model. Since a diffusion trajectory is nothing but a multichannel time series (2D or 3D, depending on the problem at hand), it should match the requirements of `mcfly`.

1. CNN architecture

The best CNN model found by `mcfly` is shown in Fig. 7. It consist of 8 convolutional layers and 2 dense ones. Except those building blocks, there are several others elements of the model: (i) activation layers which define the output of neurons given an input or set of inputs, (ii) batch normalization layers responsible for normalization of the activation of previous layers, (iii) flatten layers, which flatten the input without changing its size (required by the dense layers).

A set of hyper-parameters is required to specify a CNN model: (i) learning rate, (ii) regularization rate, (iii) number

FIG. 7. Architecture of the best performing network model found by `mcfly`.

Parameter	Values
Regularization rate	0.0008315619666385682
Number of <i>Conv</i> layers	8
Number of filters	[64, 15, 33, 43, 51, 25, 54, 35]
Learning rate	0.0027156039776859925
Hidden nodes in dense layers	1327

TABLE V. Hyper-parameters of the best performing network model shown in Fig. 7.

of *Conv* layers, (iv) number of filters in each *Conv* layer, (vi) number of hidden nodes (in dense layers). The learning rate scales the magnitude of weight updates in the training process in order to minimize the network's loss function. The regularization helps to prevent overfitting of the network. We used `mcfly`'s function `find_best_architecture` to perform a random search in the hyper-parameter space. Results for the model shown in Fig. 7 are listed in Table V.

2. Accuracy of CNN

The confusion matrix of our CNN model is shown in Fig. 8 and its performance is summarized in Table VI. Although the accuracy of the CNN is smaller than those of random forest and gradient boosting methods, the model still performs very good. It achieves the best results for the directed and anomalous modes, similarly to both feature based methods. However, the most challenging task is now the classification of the confined diffusion and not the

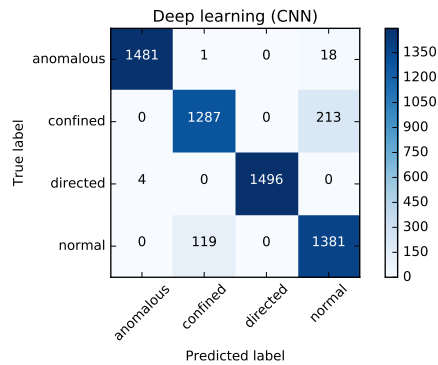


FIG. 8. Confusion matrix of the CNN classifier.

	precision	recall	support
anomalous	1.00	0.99	1500
confined	0.91	0.86	1500
directed	1.00	1.00	1500
normal	0.86	0.92	1500
average/total	0.94	0.94	6000
accuracy	94.08%		

TABLE VI. A brief summary of the performance of CNN classifier.

normal one.

C. Feature based vs deep learning

To conclude this section let us juxtapose accuracies and the processing times of the three methods analyzed in this paper. All data is collected in Table VII. Although the CNN approach is considered in many domains as the state-of-the-art method of the automatic classification, we got better results with the classical feature based methods. Moreover, they are much faster than the deep learning one. Thus, they seem to be a better choice for diffusion mode detection, even though they require more effort from human expert.

Before we abandon the deep learning approach, there is one issue to point out. In our analysis we assumed that a single trajectory corresponds to one diffusion mode. However, in reality it may happen that the motion of a particle changes its character due to some interactions with the medium. Thus, instead of classifying the whole trajectory at once it would be more desirable to divide it into short segments and then to carry out the classification separately for each segment (see e.g. Ref [25]). We mentioned already at the end of Sec. II that calculating MSD curves for short trajectories is problematic because they are limited just to a few time lags with fluctuations quickly increasing with the lag. In this case a deep learning method working with raw data only could be a better choice. We will address that issue in a forthcoming paper.

	Feature based		Deep learning
	Random forest	Gradient boosting	CNN
Accuracy	96.43%	96.97%	94.08%
Processing time	4h51min	4h22min	18h06min

TABLE VII. Comparison of all three classification methods. The processing time is understood as data preparation (if required), feature extraction (if required), searching for best performing model and finally training and validation of the classifier.

VII. CONCLUSIONS

We proposed a novel approach to analysis of SPT trajectories that makes use of convolutional neural networks, i.e. one of the popular modern deep learning methods. The biggest advantage of this approach is that it works with raw SPT data. It does not require any complex data preprocessing nor the extraction of human-engineered features from data in order to feed a classifier. Instead, it learns the features on its own from the trajectories.

Although deep learning is seen already as the state-of-the-art classification method in many areas, from our results it follows that the classical feature-based machine learning techniques like random forest or gradient boosting still outperform CNN in term of accuracy. Moreover, they are computationally cheaper (significantly shorter processing times) and much easier to interpret. For instance, they allow to rank the features according to their importance in the classification models. One should however keep in mind that we performed the whole analysis on a single CPU based workstation. Because of this we have limited ourselves to search over only 20 suitable architectures to find the best performing CNN model. Otherwise the processing times would be of the order of days instead of hours. As a consequence, the model we found is probably not the optimal one and there may be still room for improvement for the accuracy of the CNN method. Moving the whole procedure to a HPC platform would help to keep the execution times of an expanded search at an acceptable level.

The excellent performance of the traditional methods observed in our experiments may be related to the fact that we assumed the movement of the particles to be homogeneous, i.e. one generated trajectory represents a only one type of motion. In real experiments the type of the diffusion may change multiple times within one trajectory due to the interaction of the particle with the medium. To cope with that issue one usually divides the trajectory in short segments and then tries to classify each segment independently of the others. Classifiers trained on data with short lengths are required for that purpose. The CNN method could work better than the feature based ones in this case, because most of the features relate to MSD estimates that are worse (much noisier) for short trajectories.

ACKNOWLEDGMENTS

H. Loch-Olszewska and J. Szubiński were supported by NCN-DFG Beethoven Grant No. 2016/23/G/ST1/04083.

-
- [1] C. Manzo and M. F. Garcia-Parajo, Reports on Progress in Physics **78**, 124601 (2015).
 - [2] H. Shen, L. J. Tauzin, R. Baiyasi, W. Wang, N. Moringo, B. Shuang, and C. F. Landes, Chemical Reviews **117**, 7331 (2017).
 - [3] D. Holcman, N. Hoze, and Z. Schuss, Biophysical Journal **109**, 1761 (2015).
 - [4] C. Kural, H. Kim, S. Syed, G. Goshima, V. I. Gelfand, and P. R. Selvin, Science **308**, 1469 (2005).
 - [5] A. Yildiz, J. N. Forkey, S. A. McKinney, T. Ha, Y. E. Goldman, and P. R. Selvin, Science **300**, 2061 (2003).
 - [6] I. Izeddin, V. Récamier, L. Bosanac, I. I. Cissé, L. Boudarene, C. Dugast-Darzacq, F. Proux, O. Bénichou, R. Voituriez, O. Bensaude, M. Dahan, and X. Darzacq, eLife **3**, e02230 (2014).
 - [7] J. Mahowald, D. Arcizet, and D. Heinrich, ChemPhysChem **10**, 1559 (2009).
 - [8] S. B. Alves, G. F. O. Jr., L. C. Oliveira, T. P. de Silansa, M. Chevrollier, M. Oriá, and H. L. S. Cavalcante, Physica A **447**, 392 (2016).
 - [9] G. Ruan, A. Agrawal, A. I. Marcus, and S. Nie, J. Am. Chem. Soc. 2007, 129, 47, 14759-14766 (2007), 10.1021/ja074936k.
 - [10] A. M. Bannunah, D. Vllasaliu, J. Lord, and S. Stolnik, Mol. Pharmaceutics **11**, 4363 (2014).
 - [11] X. Michalet, Physical Review E **82**, 041914 (2010).
 - [12] G. R. Kneller, Journal of Chemical Physics **141**, 041105 (2014).
 - [13] N. Monnier, S.-M. Guo, M. Mori, J. He, P. Lénárt, and M. Bathe, Biophysical Journal **103**, 616 (2012).
 - [14] M. J. Saxton and K. Jacobson, Annu. Rev. Biophys. Biomol. Struct. **26**, 373 (1997).
 - [15] E. Kepten, A. Weron, G. Sikora, K. Burnecki, and Y. Garini, PLoS ONE **10**(2), e0117722 (2015).
 - [16] G. Schütz, H. Schindler, and T. Schmidt, Biophysical Journal **73**, 1073 (1997).
 - [17] R. Ferrari, A. Manfro, and W. Young, Physica D **154**, 111 (2001).
 - [18] H. Ewers, A. E. Smith, I. F. S. H. Lilie, P. Koumoutsakos, and A. Helenius, Proceedings of the National Academy of Sciences **102**, 15110 (2005).
 - [19] S. Burov, S. M. A. Tabei, T. Huynh, M. P. Murrell, L. H. Philipson, S. A. Rice, M. L. Gardel, N. F. Scherer, and A. R. Dinner, Proceedings of the National Academy of Sciences **110**, 19689 (2013).
 - [20] V. Tejedor, O. Bénichou, R. Voituriez, R. Jungmann, F. Simmel, C. Selhuber-Unkel, L. B. Oddershede, and R. Metzler, Biophysical Journal **98**, 1364 (2010).
 - [21] K. Burnecki, E. Kepten, Y. Garini, G. Sikora, and A. Weron, Scientific Reports **5**, 11306 (2015).
 - [22] R. Das, C. W. Cairo, and D. Coombs, PLOS Computational Biology **5**, 1 (2009).

- [23] P. J. Slator, C. W. Cairo, and N. J. Burroughs, PLOS ONE **10**, 1 (2015).
- [24] P. J. Slator and N. J. Burroughs, Biophysical Journal **115**, 1741 (2018).
- [25] P. Dosset, P. Rassam, L. Fernandez, C. Espenel, E. Rubinstein, E. Margeat, and P.-E. Milhiet, BMC Bioinformatics **17**, 197 (2016).
- [26] T. Wagner, A. Kroll, C. R. Haramagatti, H.-G. Lipinski, and M. Wiemann, PLoS ONE **12**(1), e0170165 (2017).
- [27] A. Krizhevsky, I. Sutskever, and G. E. Hinton, in *Proceedings of the Conference on Neural Information Processing Systems (NIPS12)* (2012) pp. 1097–1105.
- [28] K. Simonyan and A. Zisserman, “Very deep convolutional networks for large-scale image recognition,” arXiv:1409.1556.
- [29] A. Karpathy, G. Toderici, S. Shetty, T. Leung, R. Sukthankar, and L. Fei-Fei, in *Proceedings of Computer Vision and Pattern Recognition (CVPR) Conference* (2014).
- [30] L. Deng, J. Li, J.-T. Huang, K. Yao, D. Yu, F. Seide, M. Seltzer, G. Zweig, X. He, J. Williams, Y. Gong, and A. Acero, in *Proceedings of IEEE International Conference on Acoustics, Speech, and Signal Processing (ICASSP)* (2013).
- [31] A. Graves, A. Mohamed, and G. Hinton, in *Proceedings of IEEE International Conference on Acoustics, Speech, and Signal Processing (ICASSP)* (2013).
- [32] R. Collobert and J. Weston, in *Proceedings of the 25th International Conference on Machine Learning* (2008).
- [33] Y. Kim, Proceedings of the 2014 Conference on Empirical Methods in Natural Language Processing (2014), 10.3115/v1/D14-1181.
- [34] Y. Lecun, L. Bottou, Y. Bengio, and P. Haffner, Proceedings of the IEEE **86**, 2278 (1998).
- [35] Y. Zhu, Q. Ouyang, and Y. Mao, BMC Bioinformatics **18**, 348 (2017).
- [36] E. Nehme, L. E. Weiss, T. Michaeli, and Y. Shechtman, Optica **5**, 458 (2018).
- [37] M. Långkvist, L. Karlsson, and A. Loutfi, Pattern Recognition Letters **42**, 11 (2014).
- [38] X. Qiu, L. Zhang, Y. Ren, P. N. Suganthan, and G. Amaratunga, in *Proceedings of 2014 IEEE Symposium on Computational Intelligence in Ensemble Learning (CIEL)* (2014) pp. 1–6.
- [39] J. C. B. Gamboa, Computing Research Repository (2017), arXiv:1701.01887.
- [40] T. K. Ho, in *Proceedings of the Third International Conference on Document Analysis and Recognition - Volume 1* (IEEE Computer Society, 1995).
- [41] L. Breiman, Machine Learning **45**, 5 (2001).
- [42] J. H. Friedman, Comput. Stat. Data Anal. **38**, 367 (2002).
- [43] A. Fick, Annalen der Physik und Chemie (1855).
- [44] H. Freundlich and D. Krüger, Trans. Faraday Soc. **31**, 906 (1935).
- [45] F. A. Long, E. Bagley, and J. Wilkens, Journal of Chemical Physics **21**, 1412 (1953).
- [46] Y. Sagi, M. Brook, I. Almog, and N. Davidson, Phys. Rev. Lett. **108**, 093002 (2012).
- [47] I. Bronstein, Y. Israel, E. Kepten, S. Mai, Y. Shav-Tal, E. Barkai, and Y. Garini, Phys. Rev. Lett. **103**, 018102 (2009).
- [48] A. V. Weigel, B. Simon, M. M. Tamkun, and D. Krapf, Proceedings of the National Academy of Sciences **108**, 6438 (2011).
- [49] B. M. Regner, D. Vučinić, C. Domnisoru, T. M. Bartol, M. W. Hetzer, D. M. Tartakovsky, and T. J. Sejnowski, Biophysical Journal **104**, 1652 (2013).
- [50] J.-H. Jeon, N. Leijnse, L. B. Oddershede, and R. Metzler, New Journal of Physics **15**, 045011 (2013).
- [51] F. Höfling and T. Franosch, Reports on Progress in Physics **76**, 046602 (2013).
- [52] T. Bickel, Physica A **377**, 24 (2007).
- [53] M. J. Saxton, Biophysical Journal **64**, 1766 (1993).
- [54] F. Daumas, N. Destainville, C. Millot, A. Lopez, D. Dean, and L. Salomé, Biophysical Journal **84**, 356 (2003).
- [55] K. Murase, T. Fujiwara, Y. Umemura, K. Suzuki, R. Iino, H. Yamashita, M. Saito, H. Murakoshi, K. Ritchie, and A. Kusumi, Biophysical Journal **86**, 4075 (2004).
- [56] T. Kues, R. Peters, and U. Kubitscheck, Biophysical Journal **80**, 2954 (2001).
- [57] H. Salman, D. Zbaida, Y. Rabin, D. Chatenay, and M. Elbaum, Proceedings of the National Academy of Sciences **98**, 7247 (2001).
- [58] T. Bickel and R. Bruinsma, Biophysical Journal **83**, 3079 (2002).
- [59] A. Kusumi and Y. Sako, Current Opinion in Cell Biology **8**, 566 (1996).
- [60] M. J. Saxton, Biophysical Journal **67**, 2110 (1994).
- [61] M. P. Sheetz, S. Turney, H. Quian, and E. L. Elson, Nature **340**, 284 (1989).
- [62] G. H. Fredrickson, J. Phys. II (France) **5**, 369 (1995).
- [63] J. Luczka, M. Niemiec, and P. Hänggi, Phys. Rev. E **52**, 5810 (1995).
- [64] C. E. Schmidt, T. Chen, and D. A. Lauffenburger, Biophysical Journal **67**, 461 (1994).
- [65] H. Qian, M. P. Sheetz, and E. L. Elson, Biophysical Journal **60**, 910 (1991).
- [66] T. Mitchel, *Machine Learning* (McGraw-Hill Professional, 1997).
- [67] N. Hatami, Y. Gavet, and J. Debayle, in *Proceedings of SPIE, Tenth International Conference on Machine Vision (ICMV 2017)*, edited by A. Verikas, P. Radeva, D. Nikolaev, and J. Zhou (2018) p. 10696.
- [68] Y.-Y. Song and Y. LU, Shanghai Archives of Psychiatry **27**, 130 (2015).
- [69] J. R. Quinlan, Machine Learning **1**, 81 (1986).
- [70] G. James, D. Witten, T. Hastie, and R. Tibshirani, *An Introduction to Statistical Learning with Applications in R* (Springer, New York, NY, 2013).
- [71] M. Bramer, *Principles of Data Mining*, 2nd ed. (Springer Publishing Company, Incorporated, 2013).
- [72] T. K. Ho, IEEE Transactions on Pattern Analysis and Machine Intelligence **20**(8), 832 (1998).

- [73] R. E. Schapire, Y. Freund, P. Bartlett, and W. S. Lee, *Annals of Statistics* **26**, 1651 (1998).
- [74] P.-T. de Boer, D. Kroese, S. Mannor, and R. Rubinstein, *Annals of Operations Research* **134**, 19 (2005).
- [75] L. Deng and D. You, *Foundations and Trends in Signal Processing* **7**, 1 (2014).
- [76] J. B. Yang, M. N. Nguyen, P. P. San, X. L. Li, and S. Krishnaswamy, in *Proceedings of the 24th International Conference on Artificial Intelligence*, IJCAI'15 (AAAI Press, 2015) pp. 3995–4001.
- [77] M. Gardner and S. Dorling, *Atmospheric Environment* **32**, 2627 (1998).
- [78] S. Raschka, *Python Machine Learning* (Packt Publishing, 2015).
- [79] A. Papoulis and S. U. Pillai, *Probability, Random Variables, and Stochastic Processes*, 4th ed. (McGraw Hill, Boston, 2002).
- [80] L. Devroye, *Non-Uniform Random Variate Generation* (Springer-Verlag, New York, 1986).
- [81] B. B. Mandelbrot and J. W. V. Ness, *SIAM Review* **10**, 422 (1968).
- [82] C. Flynn, “FBM: Exact methods for simulating fractional brownian motion (fbm) or fractional gaussian noise (fgn) in Python.” (2017–), [Online; accessed 21-02-2019].
- [83] R. B. Davies and D. S. Harte, *Biometrika* **74**, 95 (1987).
- [84] Y. Lanoiselée, G. Briand, O. Dauchot, and D. S. Grebenkov, *Phys. Rev. E* **98**, 062112 (2018).
- [85] I. M. Tolić-Nørrelykke, E.-L. Munteanu, G. Thon, L. Oddershede, and K. Berg-Sørensen, *Phys. Rev. Lett.* **93**, 078102 (2004).
- [86] R. Metzler, J.-H. Jeon, and A. Cherstvy, *Biochimica et Biophysica Acta (BBA) - Biomembranes* **1858**, 2451 (2016).
- [87] G. V. Rossum and F. L. Drake, *Python 3 Reference Manual* (CreateSpace, Paramount, CA, 2009).
- [88] J. A. Helmuth, C. J. Burckhardt, P. Koumoutsakos, U. F. Greber, and I. F. Sbalzarini, *Journal of Structural Biology* **159**, 347 (2007).
- [89] M. J. Katz and E. B. George, *Bulletin of Mathematical Biology* **47**, 273 (1985).
- [90] D. Ernst, J. Köhler, and M. Weiss, *Phys. Chem. Chem. Phys.* **16**, 7686 (2014).
- [91] F. Pedregosa, G. Varoquaux, A. Gramfort, V. Michel, B. Thirion, O. Grisel, M. Blondel, P. Prettenhofer, R. Weiss, V. Dubourg, J. Vanderplas, A. Passos, D. Cournapeau, M. Brucher, M. Perrot, and E. Duchesnay, *Journal of Machine Learning Research* **12**, 2825 (2011).
- [92] D. van Kuppevelt, C. Meijer, V. van Hees, and M. Kuzak, “mcfly: time series classification made easy,” (2017).
- [93] J. H. Friedman, *Computational Statistics and Data Analysis* **38**, 367 (1999).
- [94] J. W. Perry, A. Kent, and M. M. Berry, *American Documentation* **6**, 242 (1955).